Search for Heavy Neutrino in $K^- \to \mu^- \nu_h(\nu_h \to \nu\gamma)$ Decay at ISTRA+ Setup

V. A. Duk [1], V. N. Bolotov, V. A. Lebedev, A. A. Khudyakov, A. I. Makarov, A. Yu. Polyarush, V. P. Novikov

Institute for Nuclear Research of RAS, Moscow, Russia

S. A. Akimenko, G. I. Britvich, A. P. Filin, A. V. Inyakin, S. A. Kholodenko, V. M. Leontiev, V. F. Obraztsov, V. A. Polyakov, V. I. Romanovsky, O. V. Stenyakin, O. G. Tchikilev, V. A. Uvarov, O. P. Yushchenko

Institute for High Energy Physics, Protvino, Russia

Abstract

Heavy neutrino ν_h with $m_h < 300MeV$ can be effectively searched for in kaon decays. We put upper limits on mixing matrix element $|U_{\mu h}|^2$ for radiatively decaying ν_h in the following parameter region: $40MeV < m_h < 80MeV; 10^{-11}sec < \tau_h < 10^{-9}sec$. The preliminary result is: $|U_{\mu h}|^2 < 6 \cdot 10^{-5}$ at $95\% C.L.$

Keywords: radiative kaon decays, heavy neutrino, sterile neutrino, LSND anomaly

1. Introduction

For more than ten years latest results of short-baselime neutrino experiments have been widely discussed and still there is no clear understanding of an event excess observed by LSND [1] and MiniBooNE [2, 3] experiments and their contradiction with KARMEN [4] results.

Oscillation interpretations of an event excess require additional sterile neutrino(s) with $\Delta m \sim 1eV^2$ (see [5] for review). An alternative interpretation of the results of all three experiments is proposed in [6]. The main idea is that in the experiments mentioned above signals from photons and electrons are indistinguishable. One could introduce heavy sterile neutrino ν_h which is produced in ν_μ neutral current (NC) interactions and decays radiatively into a photon and a light neutrino ν (decay channel $\nu_h \to \nu\gamma$ is dominant if there is large enough magnetic transition moment μ_{tr}, see [7]). In this case event excess in LSND and MiniBooNE experiments comes from photons and not from electrons. In KARMEN experiment, ν_h's with $m > 40MeV$ cannot be produced within the detector because of a threshold effect.

Combined analysis of LSND, KARMEN and MiniBooNE data results in the following properties of ν_h:

- $40MeV < m_h < 80MeV$;
- $10^{-11}sec < \tau_h < 10^{-9}sec$;

[1] Viacheslav.Duk@cern.ch

- $10^{-3} < |U_{\mu h}|^2 < 10^{-2}$.

One may consider ν_h as a component of ν_μ flavor eigenstate with the corresponding mixing matrix element $U_{\mu h}$. This leads to a very important consequence that ν_h can also be produced in charge current (CC) interactrions. If heavy neutrinos could be produced in CC interactions they can be effectively searched for in pion and kaon decays. The simplest way to do it is to study two-body decays $\pi \to \mu\nu$ and $K \to \mu\nu$ and look for a peak in muon energy distribution below the main one from $\pi \to \mu\nu_\mu$ ($\pi\mu 2$) and $K \to \mu\nu_\mu$ ($K\mu 2$). Muon energy in kaon (pion) rest frame is given by the formula:

$E_\mu = \dfrac{M_N^2 + m_\mu^2 - m_h^2}{2M_N}$ $(N = \pi, K;\ h$ stands for $\nu_h)$.

Experimental limits from $\pi\mu 2$ decay [8] were obtained for $m_h < 30MeV$: $|U_{\mu h}|^2 < 10^{-5} \div 10^{-3}$. Best limits for kaon decays come from KEK experiment [9]: $|U_{\mu h}|^2 < 10^{-4}$ for $m_h > 70MeV$. $\pi\mu 2$ decay is not sensitive to large m_h masses, while $K\mu 2$ decay is not sensitive to low m_h masses because of resolution effects and strong background from $K \to \mu\nu_\mu\gamma(K\mu 2\gamma)$ decay. Thus, a region $30MeV < m_h < 70MeV$ is not constrained at all. One should notice that these limits were obtained for relatively long-lived neutrinos flying away from a detector (photon veto was applied in both cases).

Another possibility to search for heavy neutrinos in kaon decays is to measure $K \to \mu\nu_h(\nu_h \to \nu\gamma)$ decay chain. In this case a background from $K\mu 2$ is negligible and one can obtain limits on $|U_{\mu h}|^2$ for low mass region (background from $K\mu 2\gamma$ is also small, see Chapter 7). One should stress here that only the case of radiatively decayed neutrinos is considered.

The main purpose of this paper is to search for heavy neutrino in $K^- \to \mu^-\nu_h(\nu_h \to \nu\gamma)$ with properties described in [6] and in the following parameter range: $40MeV < m_h < 80MeV$, $10^{-11}sec < \tau_h < 10^{-9}sec$.

2. ISTRA+ setup

2.1. Experimental setup

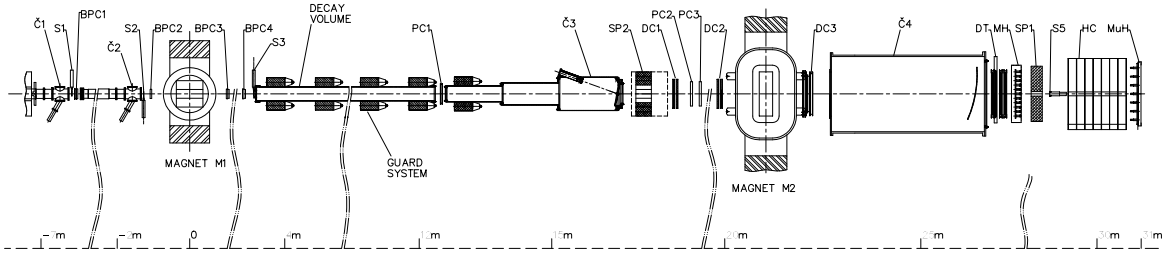

Figure 1: Elevation view of the ISTRA+ detector.

The experiment was performed at the IHEP 70 GeV proton synchrotron U-70. The experimental setup ISTRA+ (fig. 1) was described in details in [10]. The setup was located in the negative unseparated secondary beam. The beam momentum in the measurements was ~ 26 GeV with $\Delta p/p \sim 1.5\%$. The admixture of K^- in the beam was $\sim 3\%$. The beam intensity was $\sim 3 \cdot 10^6$ per 1.9 sec U-70 spill. The track of a beam particle deflected by M_1 was measured by $BPC_1 \div BPC_4$ (1mm step multiwire chambers), the kaon identification was done by $\check{C}_0 \div \check{C}_2$ threshold $\check{C}$-counters. A 9 meter long vacuum

decay volume was surrounded by 8 lead glass rings $LG_1 \div LG_8$ used to veto low energy photons. SP_2 was a lead glass calorimeter to detect/veto large angle photons. Tracks of decay products deflected in M_2 with 1Tm field integral were measured by $PC_1 \div PC_3$ (2mm step proportional chambers); $DC_1 \div DC_3$ (1cm cell drift chambers) and finally by 2cm diameter drift tubes $DT_1 \div DT_4$. Wide aperture threshold Cerenkov counters $\check{C}_3$, $\check{C}_4$ were filled with He and were not used in the measurements. Nevertheless $\check{C}_3$ was used as an extension of the decay volume. SP_1 ($ECAL$) was a 576-cell lead glass calorimeter, followed by HC ($HCAL$) - a scintillator-iron sampling hadron calorimeter. HC was subdivided into 7 longitudinal sections 7×7 cells each. MH was a 11×11 cell scintillating hodoscope used to improve the time resolution of the tracking system, MuH was a 7×7 cell muon hodoscope.

The trigger was provided by $S_1 \div S_3$, S_5 scintillation counters, $\check{C}_0 \div \check{C}_2$ Cerenkov counters, analog sum of amplitudes from the last dinodes of the SP_1 : $T_0 = S_1 \cdot S_2 \cdot S_3 \cdot \check{C}_0 \cdot \bar{\check{C}}_1 \cdot \bar{\check{C}}_2 \cdot \bar{S}_5 \cdot \Sigma(SP_1)$, here S_5 was a counter downstream the setup at the beam focus; $\Sigma(SP_1)$- a requirement for the analog sum of $ECAL$ amplitudes to be above ∼3 GeV. The last requirement served to suppress the $K \to \mu\nu$ decay. About 10% events were recorded with a different trigger: $T_1 = S_1 \cdot S_2 \cdot S_3 \cdot \check{C}_0 \cdot \bar{\check{C}}_1 \cdot \bar{\check{C}}_2 \cdot \bar{S}_5$. This prescaled trigger allowed to calculate trigger efficiency as a function of the energy released in $ECAL$.

2.2. Data and MC samples

We use high-statistics data collected in Winter 2001 run. About 332M events were stored on tapes. This statistics was complemented by 200M MC events generated with Geant3 [11]. The MC generation includes realistic description of all ISTRA+ detectors.

For signal simulation a new particle ν_h is introduced to Geant3:

- mass 40, 50, 60, 70 and 80 MeV;
- lifetime 10^{-9}, 10^{-10} and 10^{-11}sec;
- kaon is forced to decay into muon and ν_h;
- ν_h decays into a photon and a massless neutrino;
- photon angular distribution in ν_h rest frame is isotropic.

Each data sample (for certain values m and τ) containes 1M event.

3. Event reconstruction

The signature of $K^- \to \mu^-\nu_h(\nu_h \to \nu\gamma)$ is the same as for $K^- \to \mu^-\nu_\mu\gamma$. The main difference is that for $K^- \to \mu^-\nu_\mu\gamma$ it is possible to reconstruct gamma momentum in laboratory frane using the decay vertex and a shower centre while for $K^- \to \mu^-\nu_h(\nu_h \to \nu\gamma)$ the photon is emitted from secondary vertex. Nevertheless one can try to reconstruct $\vec{p}_\gamma^{lab}$ in a standard way. This allows to calculate photon momentum in the kaon rest frame but leads to an additional energy smearing (see Fig. 2).

Typical values of photon transverse momentum with respect to ν_h momentum are small, that is why smearing is not crucial. Nevertheless one could notice a slight energy shift for large τ_h.

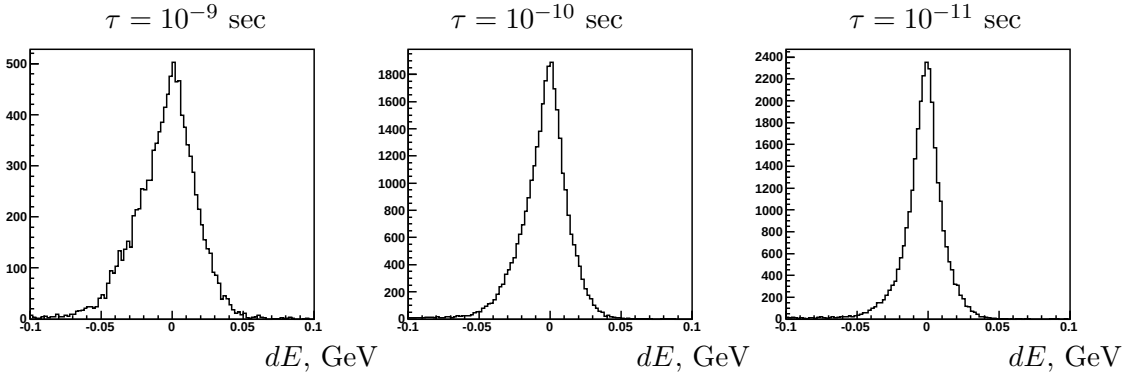

Figure 2: Photon energy smearing in kaon rest frame: $E_{measured} - E_{true}$ (MC data, $m = 60MeV$).

4. Decay kinematics

Signal distribution over muon energy in kaon rest frame E_μ has a peak similar to an ordinary $K\mu 2$ decay. So the simplest way to observe heavy neutrino is to look for a peak in E_μ.

Small transverse momentum means that photon is mostly directed along ν_h momentum in kaon rest frame. One can derive an exact formula of angular distribution:
$\frac{dN}{cos\theta} = \frac{dN}{cos\theta^\star} \cdot \frac{1}{\gamma^2(\beta cos\theta - 1)^2}$
where θ is the angle between $\vec{p_h}$ in kaon rest frame and $\vec{p}_\gamma$ in the same reference frame, $\theta^\star$ is the angle between $\vec{p_h}$ in kaon rest frame and $\vec{p}^\star_\gamma$ in ν_h rest frame, $\gamma = \frac{E_h}{m_h}$. $\frac{dN}{cos\theta^\star}$ is assumed to be constant for simplicity. In general case $\frac{dN}{cos\theta^\star} = \frac{m_\nu^2 - m_h^2}{m_\nu^2 + m_h^2}$. The last formula can be easily obtained using d-functions [16].

From the formula for angular distribution it is clear that $cos\theta \sim 1$ and hence $cos\theta_{\mu\gamma} \sim -1$ in kaon rest frame. The peak at $cos\theta_{\mu\gamma} \sim -1$ is a very good signature for the signal.

5. Primary and secondary decay vertex

The difference between z-coordinates of secondary and primary vertices is shown in Fig. 3 for different lifetimes. More illustrative is the same difference divided by the distance between primary vertex and electromagnetic calorimeter (see Fig. 4). Distribution over this ratio shows a fraction of ν_h decays within the decay volume. For $\tau_h = 10^{-11} sec$ and $\tau_h = 10^{-10} sec$ almost all neutrinos decay within an experimental setup, while for $\tau_h = 10^{-9} sec$ geometrical inefficiency becomes substantial. In Fig. 3 geometrical inefficiency could be seen as a cut-off in $dz \sim 20m$ region.

6. Event selection

Event selection for $K^- \to \mu^- \nu_h (\nu_h \to \nu\gamma)$ is very similar to that of $K^- \to \mu^- \nu_\mu \gamma$. That is why standard kinematical variables are used for the further analysis: $x = 2E_\gamma / m_K$ and $y = 2E_\mu / m_K$, E_γ and E_μ being photon and muon energies in the kaon rest frame. As in [17] Dalitz-plot will be used for studying signal and background kinematical regions.

The decay signature is defined as follows: one primary track (kaon), one negatively charged secondary track identified as muon; one shower in $ECAL$ not associated with the charged track. Muon identification using $ECAL$ and $HCAL$ is described in our previous papers ([12, 13]).

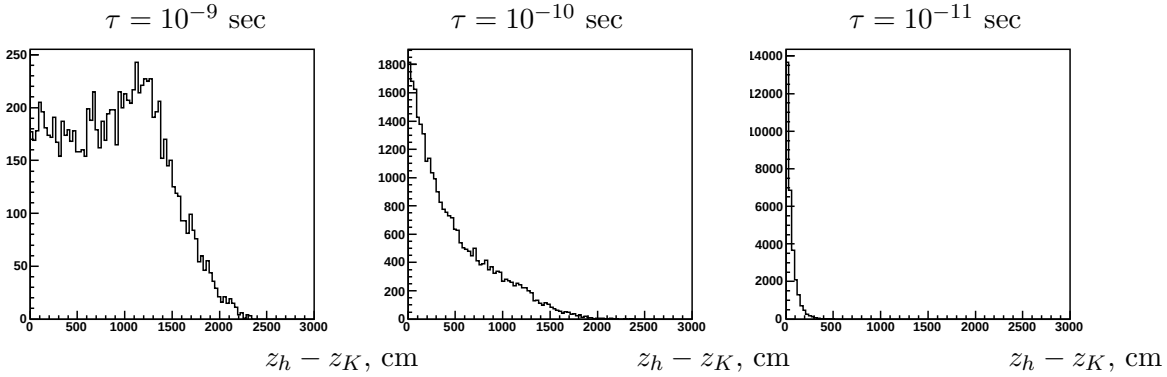

Figure 3: Difference between z-coordinates of secondary and primary decay vertices (MC, $m = 60MeV$).

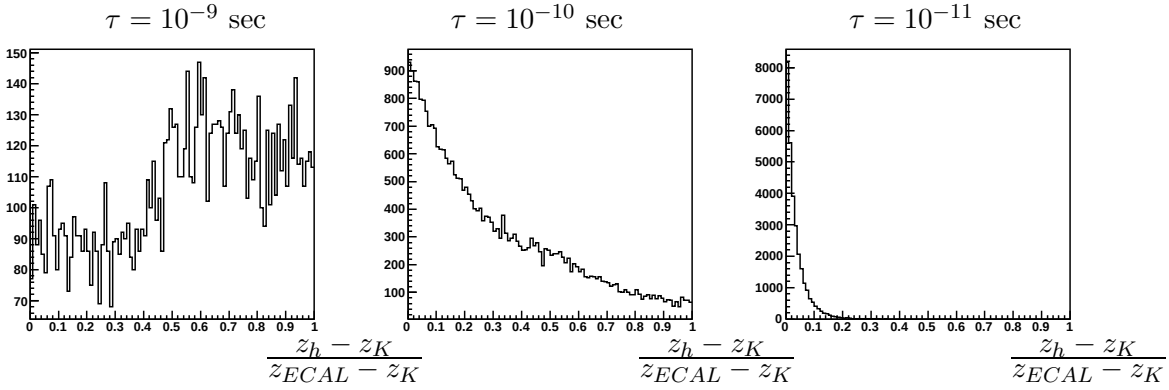

Figure 4: The same difference divided by the distance from z_K to $ECAL$ (MC, $m = 60MeV$).

Several cuts are applied to clean the data:

- number of beam and decay tracks in both X and Y projections is equal to 1;
- CL (track quality) of primary tracks in both X and Y projections must be greater than 10^{-2};
- CL of decay tracks is greater than 0.1 (decay-X) and 0.15 (decay-Y);
- the angle between primary (kaon) and secondary (muon) track is greater than 2 mrad.

The last cut eliminates most of undecayed beam particles. The quality of decay track (described quantitatively by CL) is worse than that of beam track because of multiple scattering and detector resolution.

Cuts containing photon energy include:

- gamma energy in kaon rest frame is greater than 10 MeV;
- no photons in SP_2 calorimeter (energy threshold is 0.5 GeV for total energy release);
- no photons in GS.

For vertex characteristics we have the following requirements:

- z-coordinate must be within the interval $400 < \mathrm{z}_{vtx} < 1600$cm;

- (-3) $< x_{vtx} <$ 3cm;
- (-2) $< y_{vtx} <$ 6cm;
- CL of general vertex fit is greater than 10^{-2}.

Additional cuts are applied to suppress backgrounds:

- number of hits in matrix hodoscope (MH) is less than 3;
- missing momentum $\overrightarrow{p}^{lab}_{miss} = \overrightarrow{p}^{lab}_{K} - \overrightarrow{p}^{lab}_{\mu} - \overrightarrow{p}^{lab}_{\gamma}$ does not point to the $ECAL$ central hole (this cut effectively rejects background from $K^- \to \pi^-\pi^0$ decay when the lost photon from $\pi^0 \to \gamma\gamma$ goes into the hole).

6.1. Trigger efficiency

As T_0 trigger described in Section 2 contains energy threshold in SP_1 the trigger efficiency as a function of energy released in $ECAL$ could be found using events with T_1 trigger: $\epsilon_{trg} = (T_1 \bigcap T_0)$ / T_1. Trigger curve is shown in the fig. 5. The fit is done using Fermi function. For the further analysis only events with T_0 are kept and these events are weighted by the factor of $1/\epsilon_{trg}$.

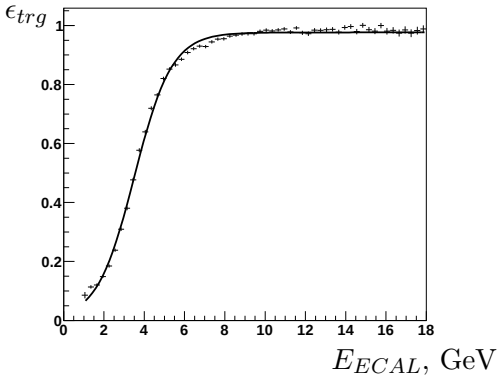

Figure 5: T_0 trigger efficiency. Points - data, curve - fit by Fermi function.

7. Signal extraction

As it was shown in Chapter 4, a peak in $cos\theta_{\mu\gamma}$ can be used for signal observation. Main background comes from 3 decay modes: $K^- \to \mu^-\nu_\mu\gamma(K\mu2\gamma)$, $K^- \to \mu^-\nu\pi^0(K\mu3)$ and $K^- \to \pi^-\pi^0(K\pi2)$ with one gamma lost from $\pi^0 \to \gamma\gamma$ for $K\mu3$, $K\pi2$ and π misidentified as μ for $K\pi2$. Dalits-plot distributions for $K\mu2\gamma$, $K\mu3$ and $K\pi2$ are shown in fig. 6, 7, 8, 9.

7.1. Signal extraction procedure

The procedure starts with dividing all kinematic (y, x) region into stripes on x (x-stripes). The x-stripe width is Δx=0.05 ($\Delta E_\gamma \sim 12MeV$). In every x-stripe we put a cut on y: $1.0 < y < 1.2$ to suppress backgrounds.

Besides distribution over cos $\theta_{\mu\gamma}$ (with a cut on y described above) we use y for the signal observation to be sure that all backgrounds are normalized properly. As in our analysis on $K\mu2\gamma$ we use simultaneous fit in x-stripes for signal extraction.

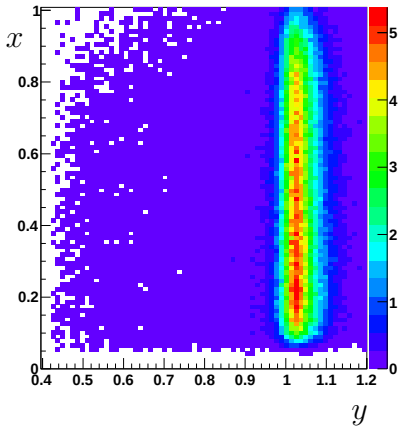

Figure 6: Dalitz-plot density for signal ($m = 60MeV$, $\tau = 10^{-10}sec$).

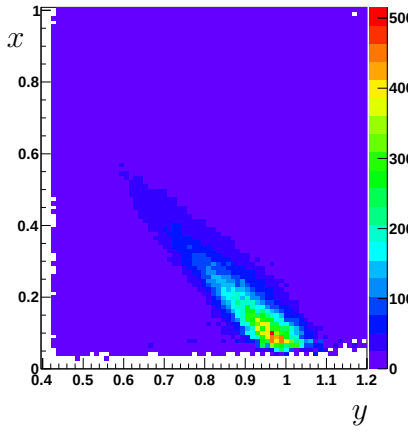

Figure 7: Dalitz-plot density for $K\mu 2\gamma(IB)$ background.

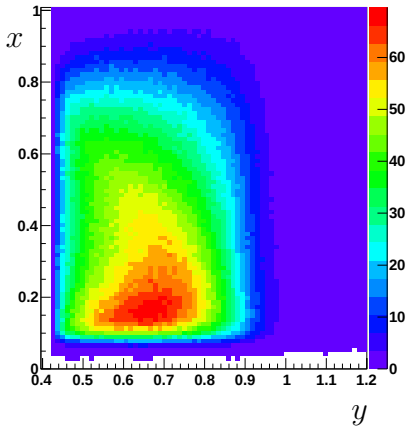

Figure 8: Dalitz-plot density for $K\mu 3$ background.

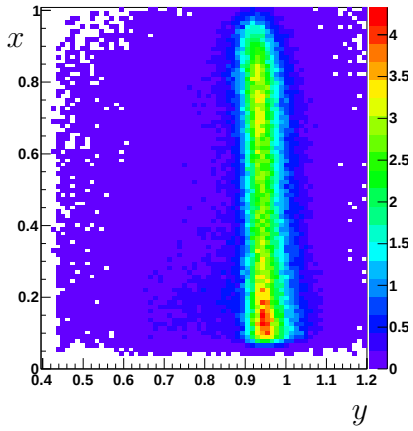

Figure 9: Dalitz-plot density for $K\pi 2$ background.

7.2. Selected kinematic region

For further analysis we have selected seven x-stripes in the following region: $0.2 < x < 0.55$ ($49MeV < E_\gamma < 136MeV$). The eighth x-stripe ($0.15 < x < 0.2$) is used for systematics study only. Experimental Dalitz-plot with selected x-stripes is shown in Fig. 10.

7.3. Possible signature for different m_h and τ

To have a feeling how the signal looks like and how sensitive our data is to heavy neutrino we plot y and $cos\theta_{\mu\gamma}$ for $m_h = 60MeV$, $\tau = 10^{-10}sec$ and $|U_{\mu h}|^2 = 10^{-2}$ in three x-stripes (Fig. 11, 12, 13, 14, 15, 16). It can be seen that $cos\theta_{\mu\gamma}$ is much better for signal observation (or setting upper limits) while y is good for reliable background normalization.

7.4. Simultaneous fit results

Results of simultaneous fits are shown in Fig. 17, 18.

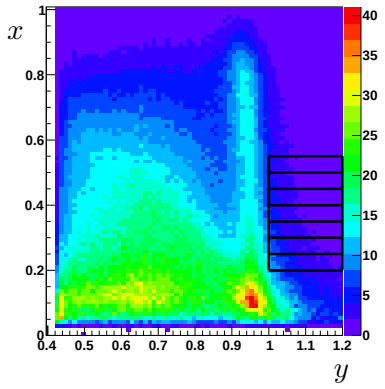

Figure 10: Dalitz-plot density for data.

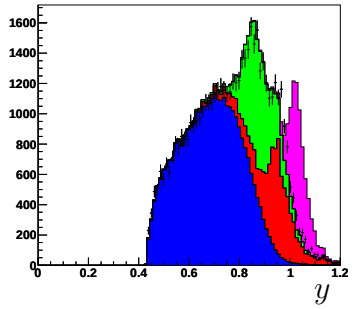

Figure 11: Data and MC. Stripe 1 ($0.2 < x < 0.25$).

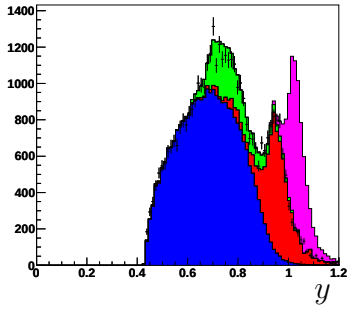

Figure 12: Data and MC. Stripe 4 ($0.35 < x < 0.4$).

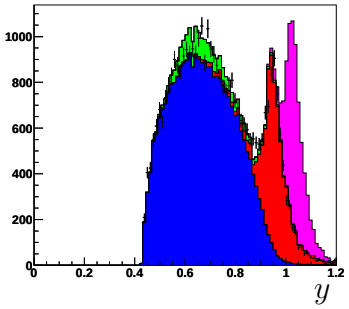

Figure 13: Data and MC. Stripe 7 ($0.5 < x < 0.55$).

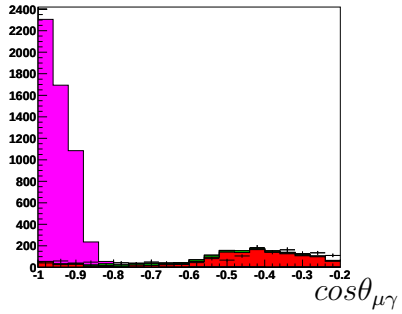

Figure 14: Data and MC. Stripe 1 ($0.2 < x < 0.25$).

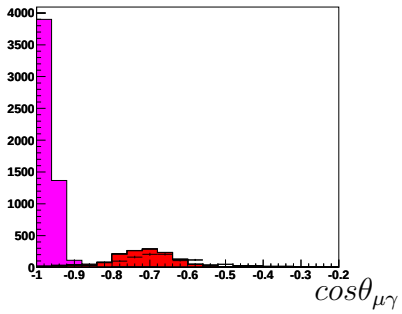

Figure 15: Data and MC. Stripe 4 ($0.35 < x < 0.4$).

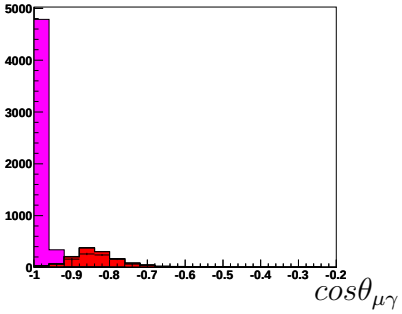

Figure 16: Data and MC. Stripe 7 ($0.5 < x < 0.55$).

Points - data, magenta - signal ($m = 60MeV, \tau = 10^{-10}sec, |U_{\mu h}|^2 = 10^{-2}$), red - $K\pi 2$, blue - $K\mu 3$, green - $K\mu 3\gamma$.

Both signal and background shapes are taken from MC. MC histograms are smoothed and the result is stored as $f(z)$ function (z= y or $cos\theta_{\mu\gamma}$). For better fit, we allow these functions to be slightly widen and shifted. We do it by using $f(k * z + b)$ instead of $f(z)$ in the fit, where fit parameters k and b are the same for signal and background and are different for y and $cos\theta_{\mu\gamma}$. For all selected x-stripes k ~1 and b ~0, i.e. our MC describes data properly (see [17] for details).

The simultaneous fit gives signal event number in each x-stripe. As we use the same data several times we should take care about correct estimation of statistical error:

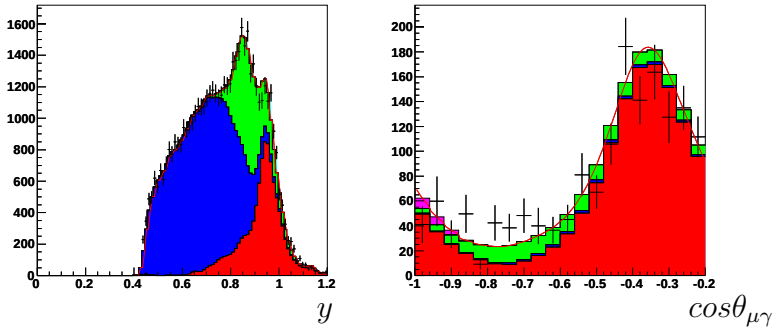

Figure 17: Simultaneous fit for m=60MeV, $\tau = 10^{-10} sec.$ Stripe 1 ($0.2 < x < 0.25$).

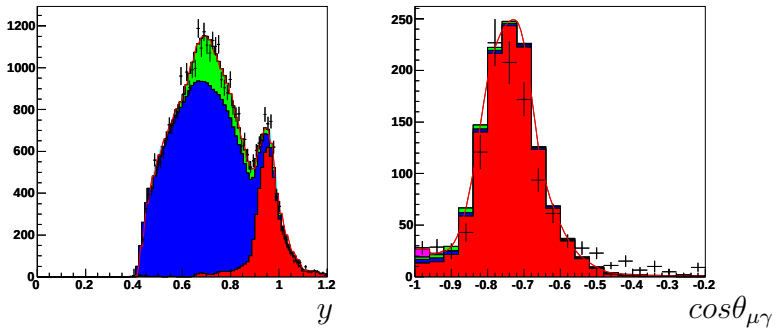

Figure 18: Simultaneous fit for m=60MeV, $\tau = 10^{-10} sec.$ Stripe 5 ($0.4 < x < 0.45$).

Points - data, magenta - signal, red - $K\pi 2$, blue - $K\mu 3$, green - $K\mu 3\gamma$.

- do simultaneous fit of two histograms and obtain $\{p_i\}$ - best parameter values (they correspond to global χ^2 minimum);
- take $\{p_i\}$ as initial values and perform χ^2/ndf and error estimation for one histogram cos $\theta^*_{\mu\gamma}$ using MINOS program [14].

8. Signal efficiency

Signal efficiency is defined as a number of events passed all cuts and kinematical selections divided by an initial event number in the same kinematical region. Distributions for different lifetimes are shown in Fig. 19, 20, 21 as a function of ν_h mass.

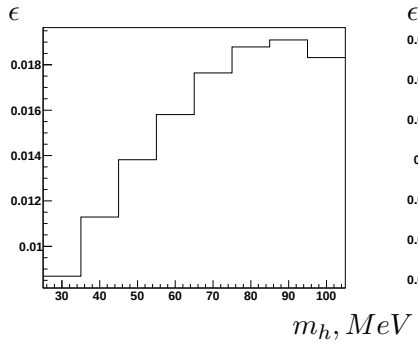

Figure 19: Signal efficiency ϵ vs ν_h mass for $\tau = 10^{-9} sec.$

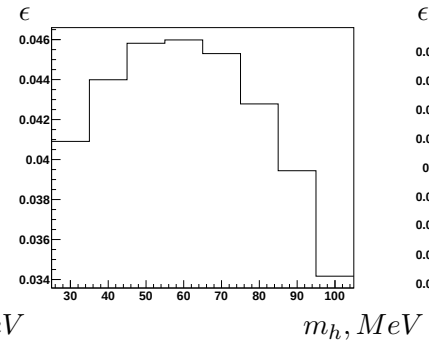

Figure 20: Signal efficiency ϵ vs ν_h mass for $\tau = 10^{-10} sec.$

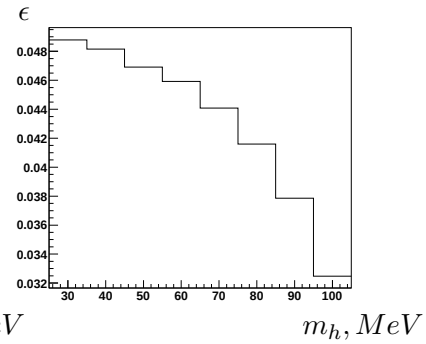

Figure 21: Signal efficiency ϵ vs ν_h mass for $\tau = 10^{-11} sec.$

Two factors influence signal efficiency:

- effective lifetime is larger for small m_h because of Lorentz boost to kaon rest frame;
- signal peak in y moves towards small muon energies for large m_h masses and is partly removed by $y > 1$ cut; it results in lower efficiency for large masses.

9. Upper limit on $|U_{\mu h}|^2$

9.1. Extraction procedure

From simultaneous fit we get $N_{exp}(\nu_h)$ for each x-stripe. This event number should be transformed to $|U_{\mu h}|^2$. This could be done either for each stripe or for all selected stripes. To avoid systematics depending on a stripe (for example backgrounds could be described worse by MC in a certain stripe and shift a total result) we use the first method.

As a normalization it is natural to use $K\mu 2\gamma$ decay. The main formula is the following:

$$\frac{N_{exp}(\nu_h)}{N_{exp}(\mu 2\gamma)} = \frac{BR(\nu_h)}{BR(\mu 2\gamma)} \frac{\epsilon(\nu_h)}{\epsilon(\mu 2\gamma)}.$$

$N_{exp}(\mu 2\gamma)$ is taken from our previous analysis in a wide kinematical region similar to signal one, $\epsilon(\nu_h)$ and $\epsilon(\mu 2\gamma)$ are efficiences obtained from Monte-Carlo. $BR(\mu 2\gamma)$ is taken from theory because experimental measurement is very old and has large error (the mean value is consistent with theoretical prediction). In future this BR could be measured at ISTRA+ setup.

$BR(\nu_h)$ is substituted by the following expression: $BR(\nu_h) = BR(K\mu 2) \cdot |U_{\mu h}|^2 \cdot f(m_h)$. Here $BR(K\mu 2)$ is taken from PDG [16], $f(m_h)$ contains chirality flip and phase space factors. It could be obtained from the general formula in [15] for meson decays to heavy neutrinos. $f(m_h)$ is dominated by chirality flip factor $1 + (\frac{m_h}{m_\mu})^2$ (see Fig. 22) and for mass interval $m_h = 40 \div 80 MeV$ it changes from 1.1 to 1.6. We assume that ν_h is a Dirac type neutrino. For Majorana type, $f(m_h)$ has an additional factor 2 and hence obtained upper limits for $|U_{\mu h}|^2$ should be divided by 2.

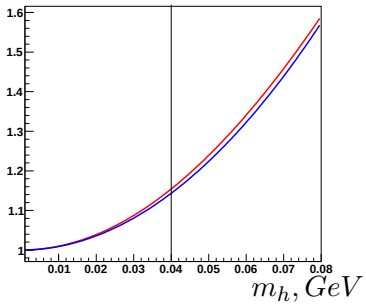

Figure 22: Factor $f(m_h)$ (red) and $(1 + \frac{m_h^2}{m_\mu^2})$(blue).

Finally we get $|U_{\mu h}|^2 \cdot f(m_h) = const \cdot \frac{N_{exp}(\nu_h)}{N_{mc}(\nu_h)}$. The last ratio in this formula is obtained directly from the simultaneous fit in an x-stripe as a fit parameter. Values $|U_{\mu h}|^2$ are calculated for all seven x-stripes (we will denote them as $|U_{\mu h}^{str}|^2$) and then averaged ($|U_{\mu h}^{av}|^2$). We call this averaging procedure a final fit.

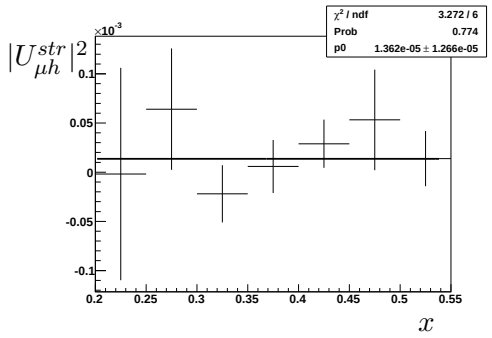

Figure 23: Final fit, m=50MeV, $\tau = 10^{-10} sec.$

The averaged value is used for UL calculation:
$U.L.(95\%C.L.) = |U_{\mu h}^{av}|^2 + 1.64 \cdot \sigma_{tot}$.

Here σ_{tot} is a total error of $|U_{\mu h}^{av}|^2$ measurement.

9.2. Extracting $|U_{\mu h}|^2$

Averaging $|U_{\mu h}^{str}|^2$ for a certain (m_h, τ_h) is shown in Fig. 23. The effect in $|U_{\mu h}^{av}|^2$ (only statistical error is considered here) does not exceed 2σ and hence an upper limit should be set.

9.3. Systematic error

Main sources of systematics are:

- fit systematics;
- cut on x (number of x-stripes in the final fit);
- cut on y in x-stripes;
- x-stripe width;
- bin size in y and $cos\theta_{\mu\gamma}$ histograms.

The largest contribution to the total systematic error comes from fit systematics caused by non-ideal shapes of a signal and backgrounds. To calculate this systematic error the following procedure is used:

- errors for $|U_{\mu h}^{str}|^2$ are scaled for each x-stripe proportionally to $\sqrt{\chi^2/n.d.f.}$;
- Averaging is repeated with these new scaled errors;
- new averaged value $|U_{\mu h}^{av,scaled}|^2$ has larger error σ_{scaled} which is treated as $\sigma_{scaled} = \sqrt{\sigma_{stat}^2 + \sigma_{syst,fit}^2}$. Here σ_{stat} is a statistical error of $|U_{\mu h}^{av}|^2$.

Systematics of a cut on x is calculated as follows:

- averaging is done for different number of x-stripes in the fit (varying cut on x);
- dependence of $|U_{\mu h}^{av}|^2$ on x is fitted by a straight line;

- a slope of this line multiplied by the x-stripe width is the estimation of systematic error.

Details of this procedure are described in [17].

9.4. Upper limits

Upper limits for different lifetimes as a function of m_h are shown in Figs 24, 25, 26. They could be compared with the region predicted in [6] (blue stripe in the Figs mentioned above).

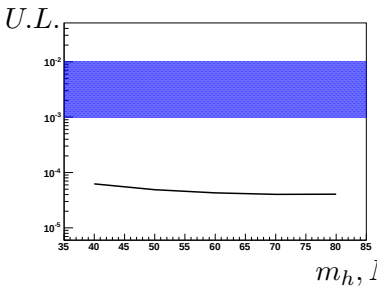

Figure 24: $\tau = 10^{-9} sec.$

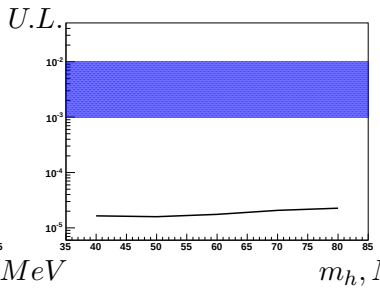

Figure 25: $\tau = 10^{-10} sec.$

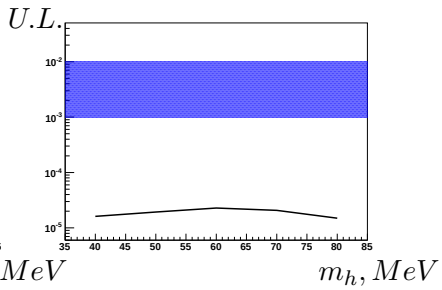

Figure 26: $\tau = 10^{-11} sec.$

Exact numbers are collected in Table 3 in 10^{-5} units.

m, MeV	$\|U_{\mu h}\|^2$	σ_{stat}	$\sigma_{syst,x}$	$\sigma_{syst,fit}$	U.L.
40	2.46394	1.53818	0.035299	1.71956	6.24808
50	1.82105	1.23596	0.0362543	1.40598	4.89171
60	1.79754	1.00459	0.00379919	1.13611	4.28471
70	1.7242	0.936114	0.000231291	1.05409	4.0362
80	1.88126	0.880383	0.0403558	0.999003	4.06604

Table 1: $\tau = 10^{-9} sec.$ Fit results and UL's in 10^{-5} units.

m, MeV	$\|U_{\mu h}\|^2$	σ_{stat}	$\sigma_{syst,x}$	$\sigma_{syst,fit}$	U.L.
40	0.63812	0.410661	0.00759285	0.461569	1.6514
50	0.660431	0.37735	0.0117351	0.426281	1.59429
60	0.733724	0.413979	0.00758282	0.46711	1.75741
70	0.977748	0.440956	0.00189752	0.504891	2.07711
80	1.05834	0.492095	0.105437	0.544141	2.27389

Table 2: $\tau = 10^{-10} sec.$ Fit results and UL's in 10^{-5} units.

m, MeV	$\|U_{\mu h}\|^2$	σ_{stat}	$\sigma_{syst,x}$	$\sigma_{syst,fit}$	U.L.
40	0.673754	0.380299	0.0167163	0.431698	1.61767
50	0.874501	0.428749	0.0344955	0.48758	1.94082
60	1.13295	0.469269	0.00850256	0.528212	2.29179
70	0.882277	0.482727	0.0762075	0.533132	2.06838
80	0.305223	0.478679	0.21034	0.50577	1.49824

Table 3: $\tau = 10^{-11} sec.$ Fit results and UL's in 10^{-5} units.

10. Conclusions

We have performed a search for a heavy neutrino in $K \to \mu\nu_h(\nu_h \to \nu\gamma)$ decay and obtained upper limits at 95% C.L. for mixing matrix element $|U_{\mu h}|^2$. The limits have been obtained for heavy neutrinos that are a part of ν_μ flavor eigenstate and decay radiatively into a light neutrino and a photon. Light neutrino mass was taken to be equal to zero and photon angular distribution in kaon rest frame was isotropic.

Upper limit at 95% C.L. for $\tau = 10^{-9} sec$ is $U.L. \sim (4 \div 6) \cdot 10^{-5}$, for $\tau = 10^{-10} sec$ $U.L. \sim (1 \div 2) \cdot 10^{-5}$ and for $\tau = 10^{-11} sec$ $U.L. \sim (1 \div 2) \cdot 10^{-5}$. Further improvements (more detailed study of systematics, more wide $m - \tau$ region, anisotropic photon angular distribution) are under inverstigation.

Authors would like to thank S.N.Gninenko, D.S.Gorbunov, V.A.Rubakov and A.A.Saratov (INR RAS) for numerous discussions. The work is supported by Russian Fund for Basic Research (grants 10-02-00330-a and 11-02-00870-a).

References

[1] A.Aguilar et al.,Phys.Rev. D64, 112007 (2001).

[2] A.A.Aguilar-Arevalo et al., Phys. Rev. Lett. 102, 101802 (2009).

[3] A.A.Aguilar-Arevalo et al., arXiv: 1007.1150 [hep-ex].

[4] B.Armbruster et al., Phys. Rev. D 65, 112001 (2002).

[5] J.Kopp, M.Maltoni, T.Schwetz, arXiv:1103.4570.

[6] S.N.Gninenko, Phys. Rev. D 83, 015015 (2011).

[7] R.N.Mohapatra, P.B.Pal, Massive neutrinos in physics and astrophysics, World Scientific, Singapore, 1991.

[8] R.Abela et al., Phys. Lett. B 105, 263 (1981).

[9] R.S.Hayano et al., Phys. Rev. Lett. 49, 1305 (1982).

[10] V.N.Bolotov et al. IHEP preprint 8-98,1998.

[11] R.Brun et al. CERN-DD/EE/84-1.

[12] I.V.Ajinenko et al. Phys.Atom.Nucl. 66(2003) 105; Yad.Fiz. 66 (2003) 107.

[13] O.P.Yushchenko et al. Phys.Lett. B581 (2004) 31.

[14] F. James, M. Roos. CERN-DD-75-20, Jul 1975.

[15] D.Gorbunov and M.Shaposhnikov, JHEP 0710, 015 (2007).

[16] K.Nakamura et al. (Particle Data Group), J. Phys. G 37, 075021 (2010).

[17] V.A.Duk et al., Phys. Lett. B 695: 59-66 (2011).